Determination of seizure propagation across microdomains using spectral measures of causality.

Ishita Basu[1], Pawel Kudela[1] and William S Anderson[1]

Abstract— **The use of microelectrode arrays to measure electrical activity from the surface of the brain is increasingly being investigated as a means to improve seizure focus localization. In this work, we determine seizure propagation across microdomains sampled by such microelectrode arrays and compare the results using two widely used frequency domain measures of causality, namely the partial directed coherence and the directed direct transfer function. We show that these two measures produce very similar propagation patterns for simulated microelectrode activity over a relatively smaller number of channels. However as the number of channels increases, partial directed coherence produces better estimates of the actual propagation pattern. Additionally, we apply these two measures to determine seizure propagation over microelectrode arrays measured from a patient undergoing intracranial monitoring for seizure focus localization and find very similar patterns which also agree with a threshold based reconstruction during seizure onset.**

I. INTRODUCTION

Electrocorticography or the recording of intracranial EEG (iEEG) involves an invasive surgical procedure for implanting electrodes directly on the exposed surface of the brain [1]. Since its development in the late 1940s as a diagnostic tool, iEEG has been used to localize epileptogenic zones and the mapping of cortical function during presurgical planning for the removal of epileptic tissue while sparing tissue involved in essential brain functions. iEEG signals are usually composed of synchronized postsynaptic potentials (local field potentials), recorded directly from the exposed surface of the cortex. These potentials may occur primarily in cortical pyramidal cells, and are conducted through several layers of tissue before reaching subdural recording electrodes placed just below the dura mater. Using depth electrodes, the local field potential (LFP) gives a measure of the neural population close to the surface of the electrode. iEEG is typically recorded over a narrow bandwidth (1-100Hz) from relatively large (1-10mm diameter), widely spaced (5-10mm) macroelectrodes. Although iEEG provides better seizure localization than scalp EEG, this technique sometimes fails to satisfactorily narrow down the seizure onset zone due to its inherent technological limitations (narrow bandwidth and 1 cm order electrode spacing). In some epilepsy centers, additional hybrid subdural recording arrays and depth electrodes are implanted for research purposes. These consist of standard subdural grid macroelectrodes mounted on the same flexible plastic substrate with microelectrode recording elements and depth electrodes with microcontacts in between pairs of macroelements (PMT Corporation, Chanhassen, MN; Ad-Tech Medical Instrument Corporation, Racine, WI).

LFP recorded using microelectrodes (micro-iEEG) in epileptic human hippocampus and neocortex has identified several new classes of electrographic activity localized to submillimeter scale tissue volumes, inaccessible to standard clinical iEEG technology [2]. Pathological high frequency oscillations have been localized to microdomains in human epileptic hippocampus [3]. Seizure like events not detectable on clinical macroelectrodes have been observed on isolated microelectrodes which were sparsely distributed, these events were more frequent in brain regions that generated seizures, and sporadically evolved into large-scale clinical seizures [2]. Microelectrode arrays embedded directly into human epileptic neocortex have shown microperiodic epileptiform discharges [4], high frequency oscillations confined to 200 mm diameter tissue regions and an ictal penumbra surrounding a core territory of recruited neurons during seizure buildup [5]. Such microelectrode arrays have also captured a detailed view of early seizure propagation in a 4×4 mm cortical region [5], [6].

Accurate seizure focus localization is of utmost importance not only for seizure management but also to avoid compromising essential brain functions. Clinical evaluation is mainly performed with visual analysis of iEEG in the low frequency (< 50 Hz) band and may result in overestimation of the seizure core territory [7]. In this work, we aim to improve seizure localization and hence minimize resection region by studying pathological evolution of seizures as captured by ictal propagation across microdomains. We fit a multivariate autoregressive model and calculate two spectral measures of causality for estimating the propagation pattern of simulated/measured epileptiform activity across 5-15 microelectrode channels.

II. METHODS

A. Simulated and patient data

The two types of data sets used were derived as follows: 1)A realistic neural network simulator (GENESIS) was used to simulate a region of cortex [8], to obtain extracellular LFPs from "virtual microelectrodes" and produce test data closely resembling multisite microelectrode recordings.The LFP for the model is derived from a weighted average of the current sources summed over the cellular compartments [9]:

$$X(\overrightarrow{r},t) = \frac{1}{4\pi\sigma}\sum_{i=1}^{n}\frac{I_i(t)}{R_i} \quad (1)$$

[1] Department of Neurosurgery, Johns Hopkins University, MD USA. Contact author: Ishita Basu ibasu2@jhmi.edu.

978-1-4244-7929-0/14/$26.00 ©2014 IEEE

where $I_i(t)$ represents an individual compartment's current, R_i is the magnitude of distance from the compartment to the recording electrode at $\overrightarrow{r}$, and σ is the homogeneous tissue conductivity. This includes synaptic currents, channel currents, and compartment currents. The cortical model used to simulate micro-iEEG, $X(\overrightarrow{r},t)$ correspond to a square area of 0.8×0.8 mm and 1.8×1.8 mm sampled by 5 and 9 microelectrodes respectively. The distance between the microelectrodes varied from 0.4 to 0.6 mm.

2)LFPs were recorded from an adult patient with intractable epilepsy who was implanted with subdural grids, strips and depth electrodes for iEEG monitoring before surgical intervention in order to localize the seizure focus and essential functional brain areas. Such patients are monitored in the epilepsy monitoring unit for 7 days or more depending on seizure occurrence. During this period, iEEG is recorded continuously along with video monitoring which is reviewed by epileptologists for seizure localization. Some of these patients consent for additional microelectrode (hybrid grids, strips, depths) implants which are currently used for research purposes. A 4×4 microelectrode grid with $40-70\mu$m diameter electrodes and a 1mm spacing between them was used. The position of the microelectrode array was decided by the treating epileptologist based on suspected seizure focus. Signals from these microelectrodes (micro-iEEG) were recorded continuously using a Blackrock Neuroport system (Blackrock Microsystems, Salt Lake City, Utah) which can record up to 128 channels at a maximum bandwidth of 30 KHz.

B. Analysis of micro-iEEG

We analyzed simulated micro-iEEG (with a known propagation pattern) and those recorded from a patient during the occurrence of symptomatic electrographic seizures which were used for localization of the seizure focus. The simulated and recorded data were sampled at 20 and 10 KHz, respectively and were down-sampled with a lowpass anti-aliasing filter to 1000 Hz. Each recorded data segment analyzed consisted of a period of $1-2$ minutes before the clinical seizure onset and ended $20-40$ s into the seizure. For the patient data, we also considered a baseline segment of a few minutes that was temporally separated from the seizure onset time and was used to estimate a null distribution for statistical analysis.

A multivariate autoregressive (MVAR) model [10] was fitted to each simulated and recorded dataset. The MVAR model for a set of M time series $X(n) = \{x_i(n)\}, i = 1,...,M; n = 1,...,N$ of length N can be described as:

$$X(n) = \sum_{j=1}^{p} A_j X(n-j) + U(n) \tag{2}$$

where, $X(n)$ is a vector of signal samples at time instant n over M channels and $U(n) = \{u_i(n)\}$ is an input vector of zero-mean white and uncorrelated noise processes with covariance matrix $\sum_U = \{\sigma_{ij}^2\}$. A_j is an $M \times M$ matrix of the model coefficients at time lag j and p is the MVAR model order.

Recorded micro-iEEG channels which were noisy or did not contain any signal were first rejected by visual inspection. An MVAR model [10] was fitted to lowpass filtered (at 50 Hz) micro-iEEG data over windows of length N starting from a few seconds before the clinical seizure onset. The model order p was chosen using a Bayesian information criterion (SBC) [11]. The number of signal samples, N were chosen by a visual inspection of the calculated SBC curves. The model parameters $A_j, j = 1,...,p$ for the simulated dataset were estimated using the Nuttall-Strand algorithm [12], whereas those for the recorded dataset were estimated using the *arfit* algorithm [13] implemented in MATLAB.

1) Propagation pattern from MVAR model: According to Grangers definition of causality [14], a time series is called causal to another time series if the knowledge of the past of the first series significantly improves prediction of the second series. The MVAR model generalizes this aspect for more than two time series signals. In the frequency domain, (2) can be expressed as:

$$X(f) = A(f)X(f) + U(f) \tag{3}$$

where $A(f) = \sum_{k=1}^{p} A_j e^{-j2\pi f \Delta t k}$ and Δt is the sampling period. The off-diagonal elements $A_{ij}(f)$ describe the dependence of x_i on the p past points of x_j at frequency$f$. Hence the presence of causal interactions between any two time series in this model is related to the presence of nonzero off-diagonal elements of the coefficient matrix $A(f)$. The presence of direct interactions between two channels can be quantified by calculating the partial directed coherence (PDC) [15]. PDC is a frequency domain measure of the directed influences between pairs of signals in a multivariate data set and quantifies the interactions from one channel to another that cannot be explained by any other observed time series. The PDC from x_j to x_i is defined as:

$$\pi_{ij}(f) = \frac{\overline{A}_{ij}(f)}{\sqrt{\sum_{m=1}^{M} |\overline{A}_{mj}(f)|^2}}; \overline{A}(f) = I - A(f) \tag{4}$$

The squared magnitude of the PDC function $\pi_{ij}(f)$ quantifies the strength of propagation from $x_j \rightarrow x_i$ at frequency f, being 0 in the absence of any flow and 1 when all causal influences originating from y_j are directed towards y_i. The calculation of PDC however does not take into account the differences in the noise variance σ_{ij}^2. To overcome this limitation, a generalized PDC (gPDC) can be defined as [16]:

$$\pi_{ij}(f) = \frac{\overline{A}_{ij}(f)/\sigma_{ii}}{\sqrt{\sum_{m=1}^{M} |\overline{A}_{mj}(f)|^2/\sigma_{mm}^2}} \tag{5}$$

where σ_{ii}^2 is the variance of the white noise process u_i. The gPDC is thus not affected by possible differences in the noise variance and quantifies direct causality from $x_j \rightarrow x_i$. (3) can be rewritten as:

$$X(f) = H(f)U(f); H(f) = (I - A(f))^{-1} \tag{6}$$

where $H(f)$ is the transfer matrix of the system and H_{ij} represents the connection between the j-th input and the i-th

output of the system. The directed transfer function (DTF) can be calculated as [10]:

$$\gamma_{ij}(f) = \frac{|H_{ij}(f)|}{\sqrt{\sum_{k=1}^{N} |H_{ik}(f)|^2}} \tag{7}$$

The DTF measure does not distinguish between direct and indirect flows, i.e. it would produce similar results for a flow between channels i and j irrespective of the presence of other channel(s) mediating the flow between them. To overcome this limitation, the direct DTF (dDTF) was introduced [17] and is defined as:

$$\zeta_{ij}(f) = \frac{|H_{ij}(f)||\chi_{ij}(f)|}{\sqrt{\sum_f \sum_{ij} |H_{ij}(f)|^2 |\chi_{ij}(f)|^2}} \tag{8}$$

where $\chi_{ij}(f)$ is the partial coherence between channels i and j. The gPDC (5) and dDTF (8) were calculated for the fitted MVAR model over a frequency band in the 1-50 Hz range .

C. Statistical analysis

The objective is to test if the values of $\pi_{ij}(f), \zeta_{ij}(f), i = 1,...,L, j = 1,...,L, i \neq j$ are significantly greater than the ones calculated from a baseline signal which is temporally separated from the seizure. Classical statistical testing approaches involving surrogates cannot be used for this case since we do not have multiple trials of the same seizure event and we want to test the presence of significant causal interactions arising during seizure initiation and propagation with respect to a baseline devoid of ictal dynamics. An empirical null distribution is estimated from values of $\pi_{ij}(f)$ and $\zeta_{ij}(f)$ in the 1-30 Hz frequency bands from overlapping baseline segments of N samples which are assumed to be devoid of ictal propagation. The values of $\pi_{ij}(f)$ and $\zeta_{ij}(f)$ in the 1-30 Hz frequency band calculated from the ictal interval of interest are then used to determine if there is any significant propagation from $j \rightarrow i$ by comparing them with the 98th percentile of the corresponding null distributions estimated from baseline segments.

III. Results

Both the simulated and recorded datasets were low pass filtered to retain frequency components below 50 Hz. The simulated dataset consisted of micro-iEEG measured from 5 and 9 microelectrodes. Both of them were fitted with an MVAR model with model order 8 and window length of 0.5 seconds (500 samples). The dDTF and gPDC were calculated and the propagation pattern was determined as shown in figures 1 and 2. In both the figures, only those connections are plotted as arrows which had a value greater than 85 percentile of the entire range of dDTF or gPDC values. Figure 1 (middle column) shows the absolute values of dDTF and gPDC over 1-30 Hz, which can be interpreted as strength of flow from the x-axis to the y-axis. It can be seen that both gPDC and dDTF reconstruct the upper right corner to lower left corner simulated flow in case of the 5 microelectrode configuration (Fig. 1). However, for the 9 microelectrode configuration, only the gPDC measure

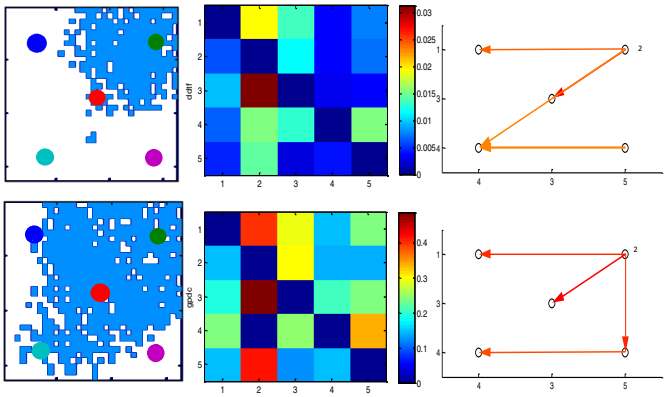

Fig. 1. Simulated micro-iEEG over a 0.8×0.8mm cortical surface measured from 5 microelectrodes shown as colored circles(left). The epileptic activity propagates from the upper right corner to the lower left corner. The values of calculated dDTF and gPDC (middle)in the 1-30 Hz frequency band was used to determine the propagation pattern (right).

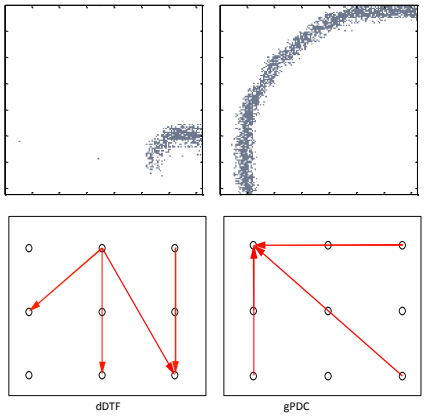

Fig. 2. Simulated micro-iEEG over a 1.8×1.8mm cortical surface measured from 9 microelectrodes (top). The epileptic activity propagates from bottom right corner to top left corner. This is correctly reconstructed by the gPDC measure (bottom right) but not the dDTF measure (bottom left).

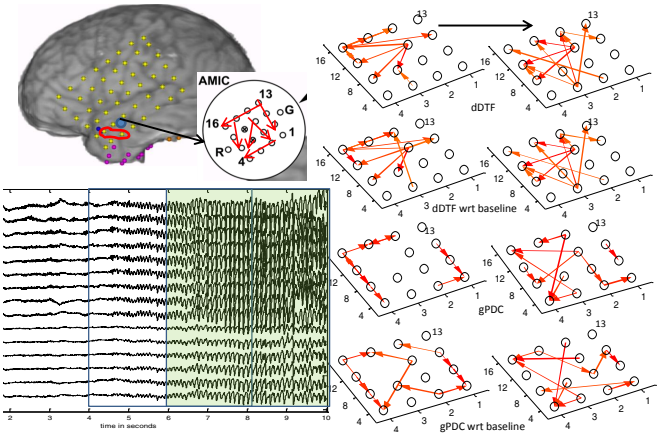

Fig. 3. Micro-iEEG recorded from a 4×4 microarray (bottom left) positioned in close proximity to the clinical seizure focus (top left). The recorded micro-iEEG were ordered by using a threshold on the amplitude of 1-30 Hz components (top left). The propagation pattern was estimated for two overlapping time windows (shown in dashed and solid boxes in the bottom left) using dDTF and gPDC measures in the 1-30 Hz frequency band (right).

correctly estimates the simulated propagation pattern from the bottom right corner to the top left corner as shown in Fig. 2. This might be due to the higher error propagation in the dDTF calculation (8) which involves a matrix inverse operation as opposed to the gPDC calculation (5).

The micro-iEEG recorded from a 4×4 microarray which was placed within a centimeter of the clinical seizure focus in a patient with intractable epilepsy was used to determine the seizure propagation pattern using the dDTF and gPDC measures. An MVAR model of order 9 was fitted to the low pass filtered 15 channels of micro-iEEG (1 noisy channel was rejected). Two overlapping 4 second time windows (shown in Fig. 3) were considered. 76 baseline segments were used to construct the null distribution of gPDC and dDTF. The propagation pattern was determined both from the absolute values of gPDC and dDTF and those which exceeded 98 percentile of the corresponding null distribution as shown on the right side of Fig. 3. Without knowledge of the underlying seizure propagation, the low pass filtered micro-iEEG traces were arranged according to the instant when their amplitude first crossed a threshold and this temporal pattern was used to reconstruct a flow pattern as shown in the bottom left of Fig. 3. It can be seen from Fig. 3 that the propagation pattern constructed by dDTF for both the time windows considered do not differ from those with respect to the baseline. The propagation estimated by gPDC has a few different flows when considered with respect to the baseline. The general flow pattern is similar for all the measures, the major difference between the two measures is that dDTF shows more flows than gPDC. This is because of the difference in normalization used in the calculation of dDTF and gPDC. While dDTF is normalized with respect to all possible flows, gPDC is normalized with respect to all flows out from a particular node. Hence, we see fewer outflows from a particular node in case of gPDC as compared to dDTF. In the first time window (4-8s), the main flow is from top right to left which is similar to that constructed by thresholding, while in the second time window (6-10s), there is an additional upwards flow.

IV. CONCLUSIONS

The results of this study indicate that frequency measures of causality that have been widely used for calculating functional connectivity of the brain [17] can be used to determine seizure propagation patterns specially over highly localized microdomains. Both the measures, dDTF and gPDC produce similar results for simulated 5 channel and recorded 15 channel micro-iEEG. However, gPDC could potentially be a more robust measure for estimating propagation patterns of these highly non-stationary and rapidly evolving micro-iEEG signals. We will be testing the performance of these two measures over more patient data sets. A major challenge with the modelling is that it is difficult to obtain multiple trials of the same event which is normally used in the calculation of functional connectivity. Future work will include estimating propagation in higher frequency ranges as well as comparing time dependent propagation patterns across microdomains inside the seizure generating region and those separated by few centimeters. We envision that a better understanding of the evolution of seizures would not only contribute to a better seizure focus localization, but would also have profound implications for early detection of a seizures. Better targeting and understanding of seizure propagation will help improve the efficacy of resection surgery as well as those of implantable anti-epileptic stimulation devices and thus lead to an improved seizure control.

REFERENCES

[1] J. Schramm and H. Clusmann, "The surgery of epilepsy," *Neurosurgery*, vol. 62, pp. SHC–463, 2008.

[2] M. Stead, M. Bower, B. H. Brinkmann, K. Lee, W. R. Marsh, F. B. Meyer, B. Litt, J. Van Gompel, and G. A. Worrell, "Microseizures and the spatiotemporal scales of human partial epilepsy," *Brain*, vol. 133, no. 9, pp. 2789–2797, 2010.

[3] G. A. Worrell, A. B. Gardner, S. M. Stead, S. Hu, S. Goerss, G. J. Cascino, F. B. Meyer, R. Marsh, and B. Litt, "High-frequency oscillations in human temporal lobe: simultaneous microwire and clinical macroelectrode recordings," *Brain*, vol. 131, no. 4, pp. 928–937, 2008.

[4] C. A. Schevon, S. K. Ng, J. Cappell, R. R. Goodman, G. McKhann Jr, A. Waziri, A. Branner, A. Sosunov, C. E. Schroeder, and R. G. Emerson, "Microphysiology of epileptiform activity in human neocortex," *Journal of clinical neurophysiology: official publication of the American Electroencephalographic Society*, vol. 25, no. 6, p. 321, 2008.

[5] C. A. Schevon, S. A. Weiss, G. McKhann Jr, R. R. Goodman, R. Yuste, R. G. Emerson, and A. J. Trevelyan, "Evidence of an inhibitory restraint of seizure activity in humans," *Nature communications*, vol. 3, p. 1060, 2012.

[6] W. Truccolo, J. A. Donoghue, L. R. Hochberg, E. N. Eskandar, J. R. Madsen, W. S. Anderson, E. N. Brown, E. Halgren, and S. S. Cash, "Single-neuron dynamics in human focal epilepsy," *Nature neuroscience*, vol. 14, no. 5, pp. 635–641, 2011.

[7] S. A. Weiss, G. P. Banks, G. M. McKhann, R. R. Goodman, R. G. Emerson, A. J. Trevelyan, and C. A. Schevon, "Ictal high frequency oscillations distinguish two types of seizure territories in humans," *Brain*, vol. 136, no. 12, pp. 3796–3808, 2013.

[8] W. S. Anderson, P. Kudela, J. Cho, G. K. Bergey, and P. J. Franaszczuk, "Studies of stimulus parameters for seizure disruption using neural network simulations," *Biological cybernetics*, vol. 97, no. 2, pp. 173–194, 2007.

[9] R. Srinivasan, S. Thorpe, and P. L. Nunez, "Top-down influences on local networks: basic theory with experimental implications," *Frontiers in computational neuroscience*, vol. 7, 2013.

[10] M. Kaminski and K. Blinowska, "A new method of the description of the information flow in the brain structures," *Biological cybernetics*, vol. 65, no. 3, pp. 203–210, 1991.

[11] H. Akaike, "A new look at the statistical model identification," *Automatic Control, IEEE Transactions on*, vol. 19, no. 6, pp. 716–723, 1974.

[12] O. Strand, "Multichannel complex maximum entropy (autoregressive) spectral analysis," *Automatic Control, IEEE Transactions on*, vol. 22, no. 4, pp. 634–640, 1977.

[13] A. Neumaier and T. Schneider, "Estimation of parameters and eigenmodes of multivariate autoregressive models," *ACM Transactions on Mathematical Software (TOMS)*, vol. 27, no. 1, pp. 27–57, 2001.

[14] C. W. Granger, "Investigating causal relations by econometric models and cross-spectral methods," *Econometrica: Journal of the Econometric Society*, pp. 424–438, 1969.

[15] L. A. Baccalá and K. Sameshima, "Partial directed coherence: a new concept in neural structure determination," *Biological cybernetics*, vol. 84, no. 6, pp. 463–474, 2001.

[16] L. Baccald *et al.*, "Generalized partial directed coherence," in *Digital Signal Processing, 2007 15th International Conference on*. IEEE, 2007, pp. 163–166.

[17] A. Korzeniewska, C. M. Crainiceanu, R. Kuś, P. J. Franaszczuk, and N. E. Crone, "Dynamics of event-related causality in brain electrical activity," *Human brain mapping*, vol. 29, no. 10, pp. 1170–1192, 2008.